New Journal of Physics

How computers can help us in creating an intuitive access to relativity

Hanns Ruder[1]**, Daniel Weiskopf**[2]**, Hans-Peter Nollert**[1]
and Thomas Müller[2]

[1] Theoretical Astrophysics, University of Tübingen, Auf der Morgenstelle 10, 72076 Tübingen, Germany
[2] VISUS (Visualization Research Center), Universität Stuttgart, Nobelstr. 15, 70569 Stuttgart, Germany
E-mail: nollert@tat.physik.uni-tuebingen.de

Abstract. Computers have added many new possibilities to the tool box used for visualizing science in general and relativity in particular. We present some new results from our own work: $(2+1)$ dimensional Minkowski diagrams showing two spatial dimensions, extended wormhole visualization, and the illustration of accretion discs by using the approximation via a rigidly rotating disc of dust. We also discuss some related examples from our earlier work, such as interactive and immersive visualization, or the visualization of the warp drive metric.

Contents

1. Introduction

Visualization of scientific concepts and results derived from them is nothing new. As far as relativity is concerned, Einstein himself [1] not only described well-known thought experiments such as that of a passenger on a train sending out light signals and comparing their propagation with that of light signals emitted by a 'stationary' light source along the tracks. He also provided graphical representations of this scene to allow the reader a more intuitive understanding of it.

Even animated visualization dates back to the early days of cinema. In 1923, the 20-minute movie 'The Einstein Theory of Relativity' [2] aimed at making a general audience familiar with the strange concepts of relativity by using animated scenes depicting various relativistic effects.

Nowadays, the use of computers has greatly increased the potential and usefulness of visualization in science, not only for the purpose of popularizing science, but also as a tool for researchers to develop an intuitive understanding of their results. In this paper, we will present examples of how the scope of visualization can be extended by employing computers and methods of computer graphics.

Visualization techniques which have already been in use for a long time can be made more complex with the help of computers, opening the possibility to demonstrate effects that could not have been shown before. Consider $(2 + 1)$ Minkoswki diagrams as an example, expanded from the familiar $(1 + 1)$ Minkowski diagrams (figure 2). In $(2 + 1)$ dimensions it becomes possible to demonstrate, e.g. aberration, effects of extended objects, objects obstructing each other or light cones intersecting with extended objects.

Second, computers allow ego-centric or first-person visualization in complex sceneries, including realistic everyday scenes. The relativistic bicycle ride through the historic part of Tübingen is a prime example for this. This particular installation has been extremely popular at museum exhibitions, science shows and similar opportunities. It has turned out that using a complex scenery which is quite familiar is much more efficient in demonstrating the effects of relativity compared to a simplified scenery built out of objects having some basic geometric shapes. If a familiar scenery is shown from the perspective of the viewer, any difference to the familiar picture becomes immediately obvious without having to go through some abstract thought process.

In general relativity, complicated space-time geometries, such as wormholes, warp drives or a Gödel universe, can be shown even from viewpoints located in strong-field regions. In addition, realistic lighting models, shadows, etc can greatly improve the overall appearance of the scene being shown and help in creating the desired intuitive impression.

Third, many physical systems, especially in astrophysics, require the use of general relativity if one wants to simulate their physical behaviour realistically [3]. Prime examples of such systems are accretion discs around black holes. The results of these simulations may then be visualized in a self-consistent way, including both the structure of the surrounding space-time and the hydrodynamics of the accretion disc. Again, a viewpoint located inside the region of interest may be chosen.

Visualizing the results of relativistic simulations is a field which still offers many challenging and exciting problems for visualization research—as opposed to the visualization of special and general relativity itself, which can be considered as state of the art, with only few open questions remaining on the level of scientific research.

Fourth, animations may be used where static images fail to evoke the desired effect. For example, a movie from the point of view of an observer moving around a $(3 + 1)$ dimensional

wormhole while watching objects travelling through the wormhole is much more efficient in conveying a mental image of the spherical shape of the wormhole than a series of still images.

Finally, computers make it possible to create interactive visualizations, allowing viewers to find their own approach to exploring a relativistic space-time. An example of this kind of installation is an interactive simulation of a black hole, where the user may place a black hole in front of several background images, choosing from black holes of different size. The background image may also come from a camera taking images of some scenery in real time.

Animations and interactive installations may also be combined with 'unusual' projection surfaces, such as immersive projections, e.g. in planetaria. Again, this is very hard to do without using computers. Immersive projection environments in particular offer the potential to engage the viewer in a much more intense way than conventional projection on flat screens.

2. Theory of special relativity

2.1. (2+1) dimensional Minkowski diagrams

Minkowski diagrams are almost as old as the theory of special relativity itself. They were introduced by the mathematician Hermann Minkowski [4], who developed and first published space-time diagrams in 1908. They carry a higher degree of abstraction than ego-centric approaches. Minkowski diagrams are still widely used in science books today since they are better suited to visualizing some aspects of special relativity which are hard or even impossible to see in ego-centric visualization.

Space-time diagrams in books can only show a static image of a fixed scenario and are usually limited to a 2D reduction of 4D space-time. With the help of computer-based rendering techniques, complex Minkowski diagrams in $(2+1)$ dimensional can be generated—quite a formidable task if it had to be done by hand. Furthermore, these diagrams can be manipulated interactively, varying parameters and navigating freely through the diagram. Finally, following the approach of multiple and coordinated views, several visualization views can be displayed simultaneously to provide a more complete picture of the physical scenario than a single visualization could.

Figure 1 shows a snapshot from a system that combines those different views for special relativistic visualization [5]. The left viewport provides a traditional 3D rendering of the static, spatial scene: cube-shaped (green) and spherical (red–orange coloured) scene objects along with a 2D cutting plane (light grey with $x-y$ coordinate axes in black) and a representation of the relativistic camera (triangle-shaped object within the blue circle). This traditional 3D scene rendering can be interactively rotated and moved to allow the user to obtain a complete picture of the 3D structure. The top-right viewport displays an ego-centric view of the relativistic camera: a visual simulation of how the fast moving observer would see the scene. (See [6] for further discussion of ego-centric visualization.) The bottom-right viewport contains the corresponding $(2+1)$ dimensional Minkowski diagram.

The $(2+1)$ dimensional Minkowski diagrams are generated automatically by taking the 3D spatial scene and reducing 3D object coordinates to 2D object coordinates by intersecting with a 2D cutting plane that defines the spatial $x-y$ coordinates of the space-time diagram. This plane can be placed and modified by the user interactively within the non-relativistic 3D view. Intersecting lines between the objects and the plane are extruded to world tubes. One point of the plane is defined as reference point of the rest frame. The relativistic camera can be placed
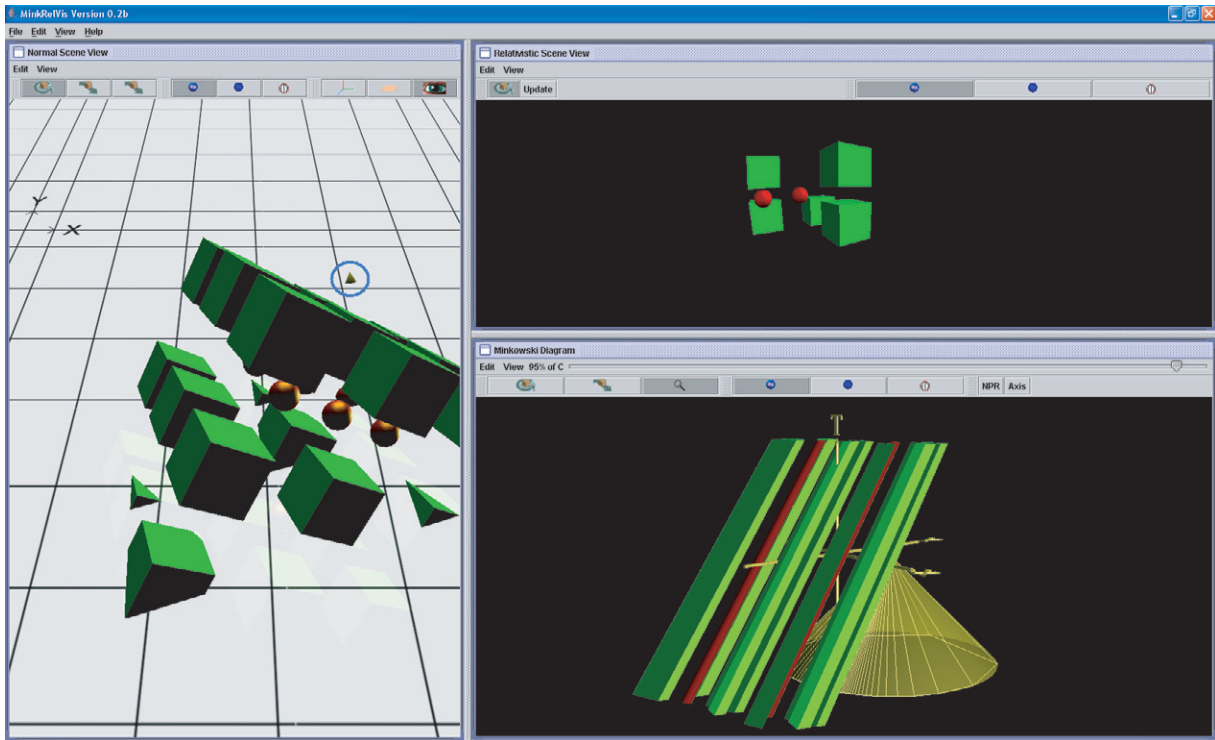
Figure 1. Multiple and coordinated views of different visualization paradigms of the same scene: (left) three-dimensional (3D) rendering of the static spatial scene, (top-right) ego-centric view from the fast moving camera, (bottom-right) the respective $(2+1)$ dimensional Minkowski diagram.

onto the plane by the user and is used as the reference point of the moving frame. The 3D rendering of the $(2+1)$ dimensional Minkowski diagram can be interactively rotated and moved to gain a full understanding of the spatial structure of the space-time diagram and to improve depth perception by motion parallax. These effects are, of course, missing in the static images of this paper.

Space-time diagrams in their $(1+1)$ dimensional form are already well suited to visualizing several fundamental effects experienced in special relativity—temporal concurrence, length contraction and causal dependency being the most important ones. In addition, $(2+1)$ dimensional diagrams can provide new information that cannot be seen in $(1+1)$ dimensional:

- Extended objects and their spatial relationships can be shown instead of simple point particles. World lines turn into world tubes.
- Visibility properties between objects can be visualized.
- Angles become apparent in two spatial dimensions.
- The aberration of light can only be seen in more than one spatial dimension.
- Objects can move in various directions of motion. In the $(1+1)$ dimensional case the direction of motion is fixed along one axis.

Therefore, the extension of $(1+1)$ dimensional to $(2+1)$ dimensional Minkowski diagrams yields a significant increase in information content. Interestingly, the step to a complete
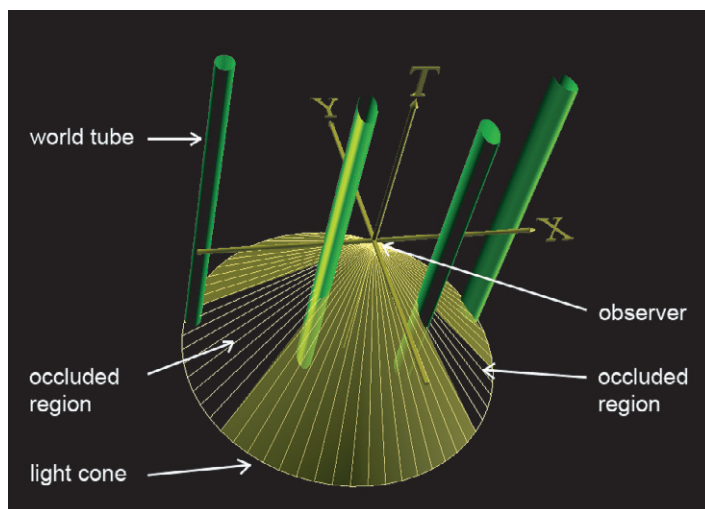
Figure 2. Visualization of a $(2+1)$ dimensional Minkowski diagram, showing x, y and t coordinate axes, the observer on top of the backward light cone, as well as world tubes of the scene objects.

$(3+1)$ dimensional representation lacks a comparable qualitative enhancement: the full 3D spatial domain can be sampled by rotating a 2D spatial plane around the direction of motion of the observer; due to the cylindrical symmetry of the Lorentz transformation with respect to this axis of rotation, any orientation of the plane gives the same qualitative picture.

Figure 2 illustrates how $(2+1)$ dimensional diagrams can be displayed. Orthogonal axes are drawn for the x, y and t dimensions. The observer (i.e. relativistic camera) is placed at the head of the backward light cone, which is rendered yellow and textured by lines originating from the observer. World tubes are represented by the boundary surfaces originating from the extrusion of the outlines from the intersection of the extended 3D spatial objects; the world tubes are coloured the same as their counterparts from the 3D spatial scene. Occlusion of one spatial object by another spatial object conveys visibility properties. Occluded regions are indicated by removing the yellow shading of the light cone in those regions; only the lines originating from the observer are still shown. Figure 2 illustrates the visualization of occlusion via shading, and figure 3 highlights this kind of visualization by comparing it with an image that does not explicitly show occluded regions.

Figure 4 adopts the Minkowski diagram of figure 3, where the observer is at rest relative to the scene objects, and applies different relative velocities. The observer is at rest in the Minkowski diagrams. The scene objects move along the y-axis. Therefore, the world tubes, which are parallel to the t-axis in figure 3, are tilted with growing angle for increasing speed in figure 4. The variation of relative velocity leads to different angles of intersection between the backward light cone and the world tubes; the angles shift towards the negative y-axis (which is the direction of motion of the observer), illustrating the effect of relativistic aberration of light. The aberration is additionally visualized by the yellow lines on the light cone: the lines are isotropic for the observer at rest (figure 3) and get compressed along the negative y-axis for increasing speed. Figures 3 and 4 also demonstrate that the visibility properties are invariant under Lorentz transformations: regardless of the observer's speed, the leftmost world tube is occluded by the second leftmost world tube in the same way in all space-time diagrams.
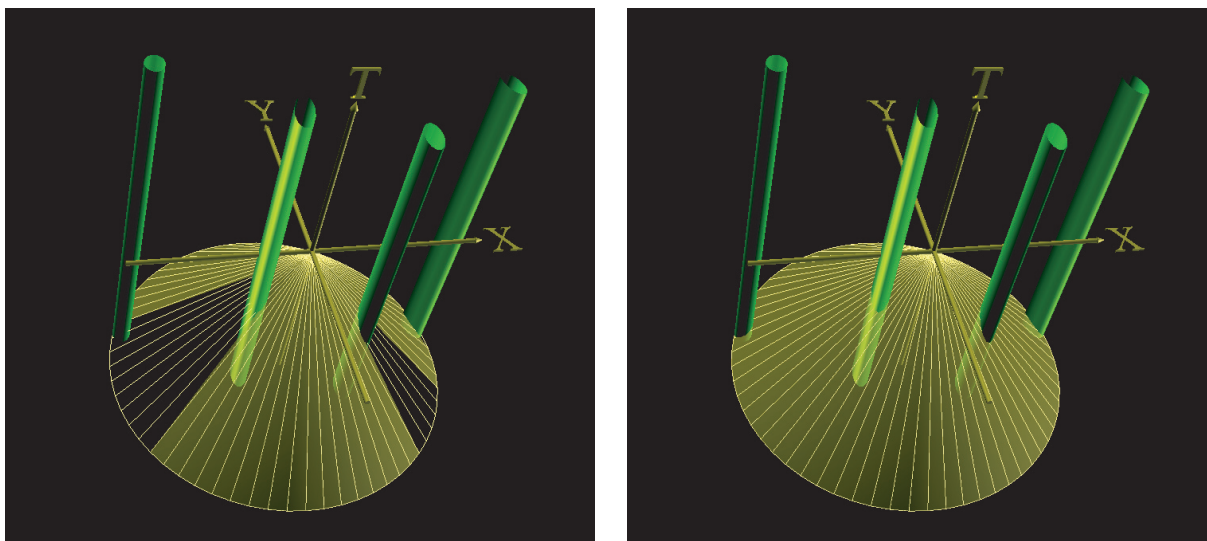
Figure 3. Visualizing visibility and occlusion: (left) occluded regions are visualized by removing the yellow shading of the light cone; (right) for comparison, no visualization of occlusion. Both pictures show the observer at rest relative to the scene objects (relative speed $\beta = 0$).
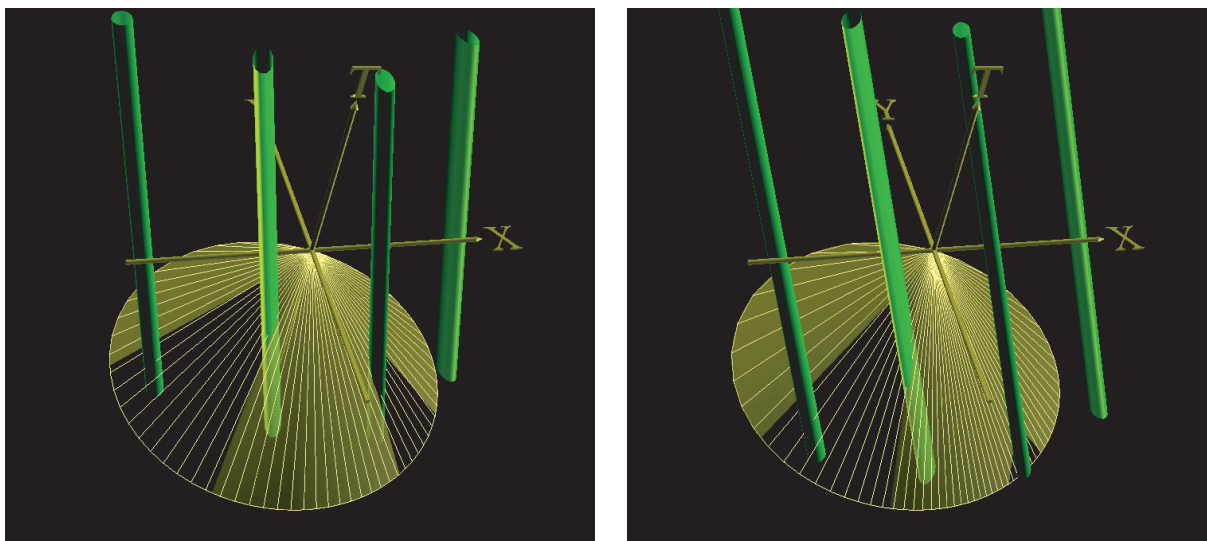

Figure 4. Varying relative velocity: (left) $\beta = 0.4$, (right) $\beta = 0.75$.

Current work on $(2+1)$ dimensional Minkowski diagrams focuses on the user interface, especially with respect to 3D navigation. This is a fairly complex issue since all three different views offered by the program have to be based on different spatial models.

2.2. First-person perspective: interactive and immersive installations

In the last section, we have seen three different approaches to visualizing not only special relativity scenes, but just about any scientific theory applied to some system which is not

Figure 5. Three-dimensional model of the old town of Tübingen.

easily accessible to our natural senses: 3D rendering of a static spatial scene as seen from the outside, ego-centric view from a moving camera and Minkowski diagrams in $(1+1)$ or $(2+1)$ dimensions. Naturally, the ego-centric approach is especially well suited for presentations to the general public, and often also particularly impressive and enjoyable to the scientist. The remainder of this paper is therefore mostly devoted to this approach. An exhaustive discussion of its potential is, however, well beyond the scope of this paper. The interested reader may turn to an in-depth review by Weiskopf *et al* [7], whereas we will only present a few instructive examples here.

Interactive installations are particularly well suited for the purpose of public outreach. Offering a playful, low-threshold introduction, they are very inviting and motivating for a first approach to the world of special relativity.

Taking advantage of an extremely detailed and realistic 3D model of large parts of the old town of Tübingen [8] (figure 5) the user can go on a virtual tour using a joystick for navigating and controlling speed [9]. To make the experience more realistic, a modified exercise bike can be used instead of the joystick (figure 6). Speed is now determined by how fast the cyclist is pedalling, direction is controlled by the handlebars. The scenery is projected onto a screen in front of the cyclist. Giving the screen some curvature adds a somewhat immersive character to the experience, creating a more realistic feeling.

Particularly instructive are 360° panoramic images of relativistic motion from a first-person perspective. Figure 7 demonstrates how aberration leads to a pronounced difference between the forward and backward direction, with the forward direction showing an effect like that of a wide-angle lens and a telephoto appearance in the backward direction; towards the sides the distortion of objects is most prominent. The next step after panoramic images is the projection in an immersive environment, such as a planetarium dome (figure 8).

Only the geometric distortions resulting from Lorentz contraction and aberration are included in figures 7 and 8. In addition, aberration also contributes to the so-called searchlight

Figure 6. Taking a bicycle ride through Tübingen up to nearly the speed of light (reduced to a virtual value of $30 \, \text{km} \, \text{h}^{-1}$). Image reprinted from Weiskopf *et al* [7], © 2006 IEEE.

Figure 7. Bottom: panoramic image of the view experienced by an observer moving at relativistic speed across the market place in Tübingen. Top: view at rest for comparisony. Image reprinted from Nollert *et al* [10].

effect shown in figure 9: in the direction of motion, the image becomes much brighter than anywhere else. This is a consequence of light coming in from all directions becoming shifted towards the forward direction by aberration. In addition, radiation coming from this direction is blue-shifted and thus carries more energy.

Finally, there is the familiar Doppler effect shifting the frequency of light up, if one is approaching the source of radiation, or down, if one is moving away from it. The overall effect, however, is not as simple as making an image look bluish in the forward and reddish in the backward direction. The final colour impression depends on the spectral properties of the source

Figure 8. Image covering half a sphere (2π) for projection on a planetarium dome. This is a still image from a movie showing the bicycle ride through Tübingen.
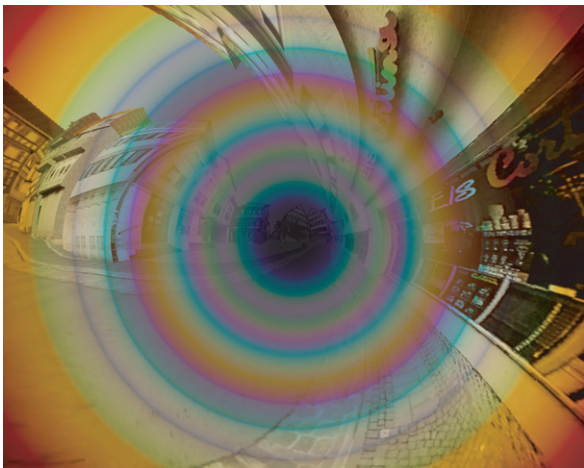

Figure 9. Left: Doppler effect resulting from motion at a velocity of 95% of the speed of light. Right: searchlight effect at the same velocity. Image reprinted from Nollert *et al* [10].

in a range much wider than just the visible part. For a realistic representation of the Doppler effect, one needs to know the emission spectrum of a light source far into the infrared and ultraviolet range since these may be shifted into the visible range by the Doppler shift. This presents a problem since for most objects, no information is available outside the visible part of the spectrum. In creating figure 9, we approximated the spectrum as a Planck spectrum; this is probably not realistic.

Figure 9 also demonstrates that including Doppler and searchlight effects tends to cover up the geometric distortions, the images becoming more confusing overall. Therefore we usually reserve them for a few dedicated pictures, including only the geometric effects in most pictures.

A variation of the scheme of interactive relativistic travel is a relativistic flight simulator [11]. It is based on an interactive simulation program which is used widely to practice the control of model airplanes. As a special option the display may be changed to a realistic view from the cockpit for movement at relativistic speed.

3. Theory of general relativity

The most obvious visual effect of special relativity is an apparent distortion of objects moving at velocities near the speed of light. In general relativity, on the other hand, the dominating topic is the real distortion of space-time or, rather, the geometry of space-time which is usually non-Euclidean.

It is all but impossible to imagine curved space-time. Thus, all visualization work in general relativity is fraught with this very problem. A common strategy to deal with this difficulty is to reduce the number of dimensions to two, and then draw an embedding of the geometry of a 2D surface in 3D Euclidean space. This approach can be very helpful and instructive, but it has several drawbacks: the level of abstraction is rather high, which is not a problem within the scientific community, but it makes embedding diagrams difficult to use for the purpose of popularizing science. The number of dimensions must be reduced, usually to two spatial dimensions. This not only suppresses the third spatial dimension, it also limits the presentation to static space-times.

Again, an alternative made possible by the use of computer graphics lies in first-person visualization, that is, showing what an observer would see in a certain situation. No reduction of dimensions is necessary, and time-dependent space-times may be shown as well. It is also possible to include interactive control by the viewer.

Just as in special relativity, the end result depends mostly on properties of light rays. In special relativity, aberration is the major cause of unexpected visual effects. In general relativity, the null geodesics in the space-time between the source of the light and the observer determines what one sees.

We will show examples of two types of space-times: wormholes [12], both non-rotating and rotating, and warp drive bubbles [13]. While these may be considered somewhat exotic, they present special challenges for their visualization and offer the potential for outstanding visual results.

3.1. Wormholes

The major difficulty encountered in visualizing wormhole geometries lies in creating the impression of a spherical structure, rather than that of a tunnel or a tube. This may be due
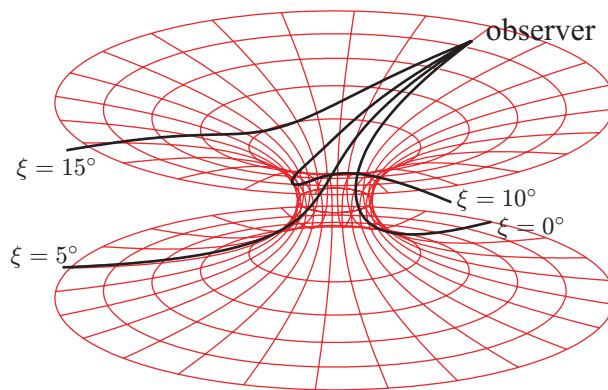
Figure 10. Null geodesics in a Morris–Thorne wormhole space-time: light rays separated by $\Delta\xi = 5°$ (where $\xi = 0$ denotes the radial direction) in the observer's frame may originate from the same side or from the other side of the wormhole.
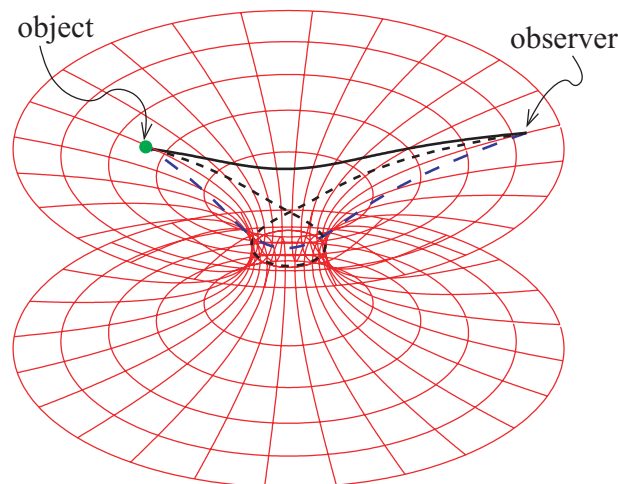
Figure 11. Light from the same object may reach an observer via infinitely many different paths. Here, we show light rays responsible for the images of first-order (black solid line), second-order (blue dashed line), and third-order (black dashed line).

to the general difficulty in imagining distorted 3D geometries, compounded by the fact that a wormhole space-time has a topology which is different from that of Euclidean space. Also, a wormhole is often presented as a connection between different regions of space in the same space-time or between space-times which are otherwise disconnected. This also suggests an image of a tunnel or a tube.

This wrong imagination is also reinforced by the kind of embedding diagram that is often shown to illustrate a wormhole, with the common practice of suppressing one spatial dimension (figures 10 and 11). While such embedding diagrams are formally correct and actually quite useful for deriving and explaining the behaviour of objects or light in such a space-time, they still inspire the wrong intuition of tube-like structures.
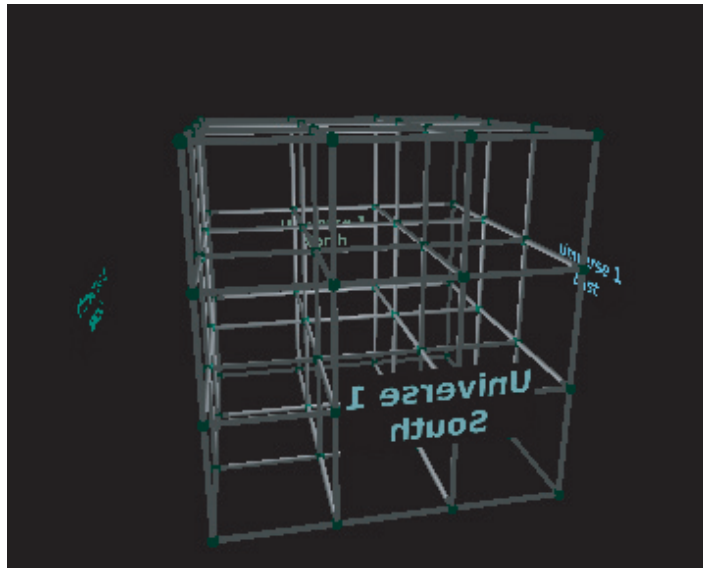
Figure 12. Undistorted lattice with four signs showing the four directions of the compass for orientation.

Figure 13. The observer is located at $l = 13$ and has a field of view of $60° \times 48°$. A wormhole throat opens in the middle of the lattice structure. The size of the throat increases (from left to right) from $b_0 = 0$ to $b_0 = 0.5$ and $b_0 = 2.0$.

In this section, we use a simple form of a wormhole, discussed by Morris and Thorne [12]. It has the metric

$$ds^2 = -c^2 dt^2 + dl^2 + (b_0^2 + l^2)(d\vartheta^2 + \sin^2 \vartheta \, d\varphi^2). \tag{1}$$

Coordinate time t is a global time coordinate for this space-time. The Morris–Thorne metric is spherically symmetric. A minimal surface $A_{\min} = 4\pi b_0^2$ at $l = 0$ marks the throat of the wormhole.

Figures 13 and 14 show how surrounding the wormhole with a grid-like structure (figure 12) helps to create the impression of the wormhole being a spherical structure [14]. Adding illumination further improves the 3D appearance of the scene. For simplicity, the illumination in these figures is realized in a 3D Euclidean space, the illuminated beams of the lattice are then placed in the wormhole geometry. A movie showing the scene from the point of view of an observer who circles the wormhole has an even stronger effect[3]. The series of

---

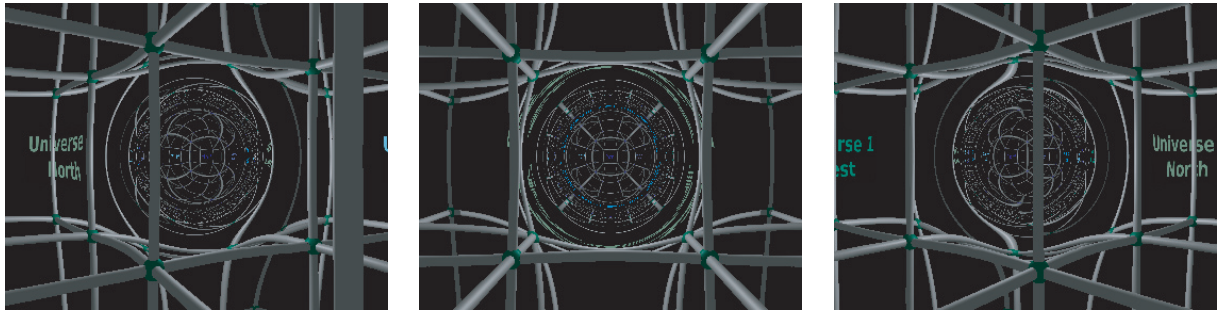[3] WHGrid.mp4, available from stacks.iop.org/NJP/10/125014/mmedia.
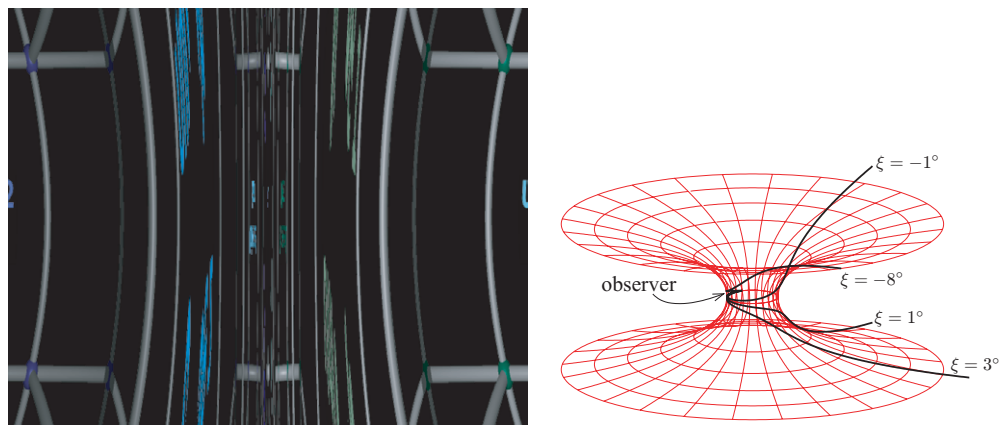
Figure 14. Moving around the wormhole.

Figure 15. The observer is located at the wormhole throat ($l = 0$), looking along the ∂_φ direction. ξ marks the angle with respect to the ∂_φ direction in the observer's frame of reference.
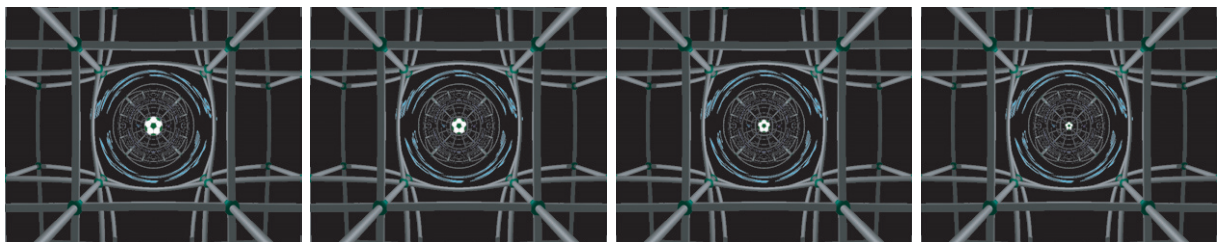

Figure 16. A soccer ball is thrown from the observer's position towards the center of the wormhole (i.e. towards its center of symmetry).

images in figure 14 conveys similar information but with a less immediate and intuitive effect. Figure 15 depicts the situation where a traveller looks along the ∂_φ-direction, perpendicular to the direction of motion, from a point located on the throat of the wormhole.

Figure 16 shows a soccer ball being thrown towards the centre of the wormhole (i.e. its centre of symmetry) from the position of the observer. Not surprisingly, it is seen moving straight away from the observer. Incidentally, this would look the same if the ball was not thrown towards the centre of the wormhole, but at an angle to this direction. The reason is that in any
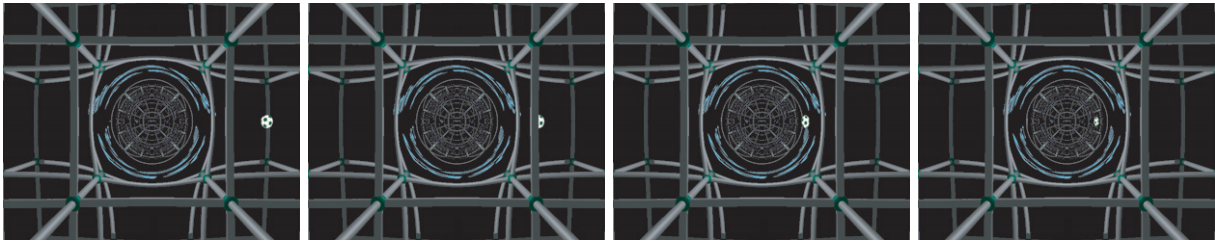
Figure 17. A soccer ball is thrown towards the center of the wormhole (i.e. towards its center of symmetry) from a point to the right of the observer.
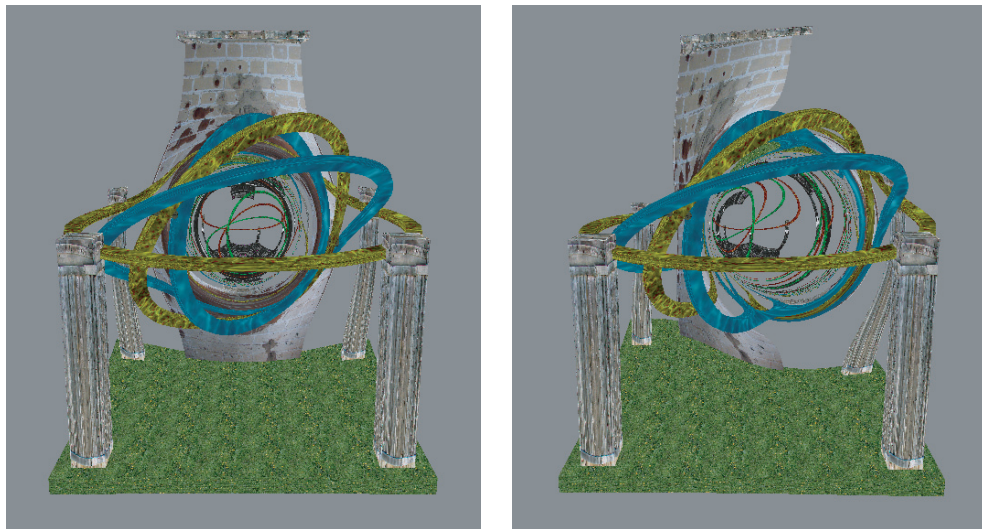

Figure 18. Hypothetical machine creating a traversable non-rotating Morris–Thorne wormhole (left) and a rotating wormhole (right).

space-time where the (tt) component of the metric is constant, the spatial projection of time-like geodesics are identical to those of null geodesics with the same initial conditions.

In figure 17, a ball is thrown towards the centre of the wormhole from a point towards the right of the observer. It does not move across to the left side of the picture, but remains on the right side while travelling through the wormhole. This behaviour can be immediately understood by drawing its world line on an embedding diagram such as figure 10.

These sequences are available in animated form[4].

A Morris–Thorne wormhole has no angular momentum, but it may be generalized to describe a rotating wormhole in a way similar to going from a Schwarzschild metric to a Kerr metric [15]. Figure 18 shows a hypothetical machine creating a non-rotating Morris–Thorne wormhole and another one for a rotating wormhole. A rotating wormhole may contain an ergoregion [15]. Even more interesting for someone passing through may be the fact that the exotic matter which is necessary for stabilizing any traversable wormhole need not be distributed evenly around the throat, as it has to be for a non-rotating wormhole. Therefore there may be trajectories through the wormhole which do not touch exotic matter.

---

[4] MTballcent.mp4 and MTballright.mp4, available from stacks.iop.org/NJP/10/125014/mmedia.

Figure 19. Screen shot: interactive wormhole connecting Tübingen and Stuttgart (360° panoramic image).

3.1.1. Interactive visualization of wormhole geometries. Since wormholes have a structure more complex than that of a 'simple' black hole, an interactive tool, allowing the user to navigate a wormhole space-time at will, could be quite helpful in gaining an intuitive understanding of its geometry. So far, this can be realized only for non-rotating wormholes, provided that no objects are located near the throat, e.g. an isolated wormhole in space with distant stars or galaxies as a backdrop.

In this case, the null geodesics can be computed ahead of time and stored as a mapping from the distant background to the camera image. Any movement of a camera on an observer at constant radius from the center of the wormhole is then equivalent to a rotation of the background image. If the movement changes this distance, the null geodesics have to be recomputed, but this can be done efficiently on the graphics processor, provided that no other objects are near the wormhole. Figure 19 shows a screen shot of a program implementing this method for a non-rotating wormhole.

If, on the other hand, objects are present near the throat, then intersections of light rays with these objects need to be determined for the specific location of the observer and of all objects in the scene. Therefore, all null geodesics reaching the observer have to be re-computed for every new location of observer and objects. This cannot yet be achieved at sufficient resolution and frame rate. This is rather unfortunate, since placing objects in the vicinity of the throat greatly helps in visualizing the effects of the wormhole geometry. Probably increases in CPU power as well as memory capacity by several factors of 10 are needed to realize a high-quality interactive visualization of wormholes which allows the inclusion of arbitrary objects.

3.2. Warp drive bubbles

Another example of an exotic space-time which is permitted in general relativity is the warp drive geometry [13]. In such a geometry one may consider a limited part of space as the inside
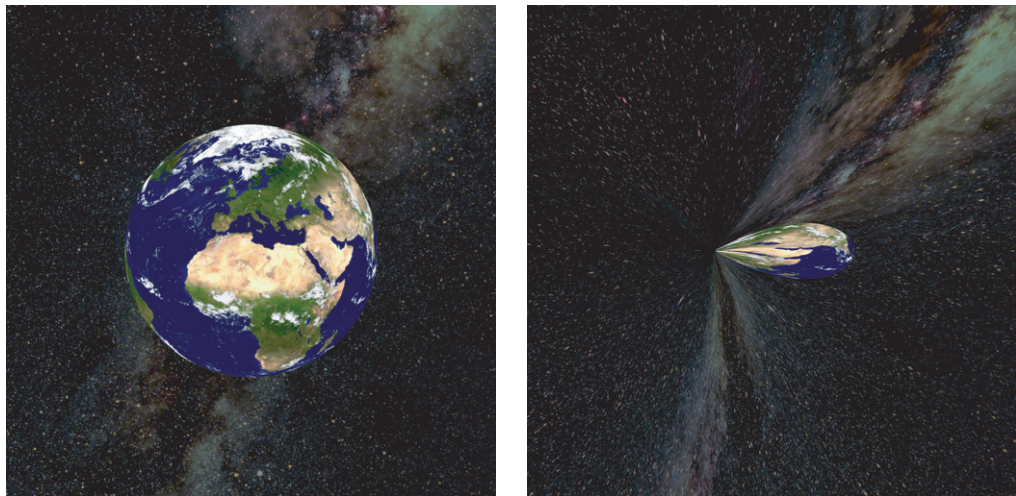
Figure 20. View from inside a warp bubble. Left: approaching the Earth, looking forward. Right: moving away from the Earth, looking backward. Image reprinted from Nollert *et al* [10].

of a warp bubble, separated from the outside by the walls of the bubble. The bubble may be moved around by compressing space in front of the inside part while stretching it in the back. There is no limit for the speed of this distortion. One can now imagine that a spaceship may be placed inside the bubble, thereby moving it from one part of the universe to another at any desired speed. No acceleration is felt inside the bubble, and the proper time inside does not differ significantly from the proper time at infinity.

Just like traversable wormholes, warp drives require considerable amounts of exotic matter and are therefore unlikely to be realized in nature or as a result of technological activities. Nevertheless, they provide a welcome opportunity for fascinating visualizations, especially since they are also quite popular with a general audience.

Looking forward from inside the warp bubble, hardly any distortion is discernible (figure 20, left panel). In the backward direction, the receding earth appears strongly distorted (figure 20, right panel). This distortion is centred on a point in the exact backward direction; the distortion quickly fades for an increasing angle between the line of sight and the backward direction.

More exciting visual effects are obtained if a warp bubble moves between the observer and some object. In figure 21, both the Earth and the Moon as well as the observer are located far enough from the warp bubble to feel no actual distortion of the local geometry due to the bubble.

3.3. Discs in relativistic astrophysics

Wormholes and warp drives, though not prohibited by the theory of general relativity, are now, and will likely continue to be, of a purely theoretical nature. We will now move back closer to physics, by turning to the visualization of the results of computer simulations in astrophysics, specifically of accretion discs in the neighbourhood of black holes.

Most, if not all, galaxies have a black hole at the center. While there is no direct observational evidence for accretion discs around these black holes, they are almost inevitable

Figure 21. A spaceship inside a warp bubble moves past between the observer and the Earth–Moon system. Image reprinted from Nollert *et al* [10].
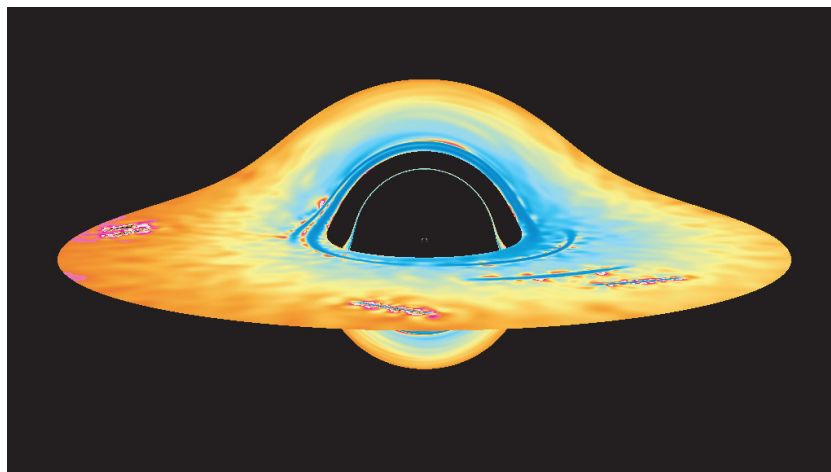

Figure 22. Visualization of an accretion disc around a black hole. Colours correspond to temperatures on the surface of the disc. The hydrodynamics equations are solved using an SPH code in a Newtonian space-time. The differences from a fully relativistic simulation are probably small enough to be hardly visible in a picture like this. Image reprinted from Nollert *et al* [10].

due to the angular momentum of matter falling towards a black hole. Simulating an accretion disc around a black hole is a formidable problem, combining challenges of numerical hydrodynamics with those of numerical relativity. It is possible now to perform a hydrodynamical simulation on the fixed background metric of a black hole. The task of creating a self-consistent model which includes the disc as a source in the Einstein field equations has not been completed yet.

There are several different approaches to go about solving the hydrodynamics equations. In the context of accretion discs, the formalism of smoothed particle hydrodynamics (SPH) has the advantage of not requiring the explicit formulation of a boundary condition. Figure 22 shows the result of a 2D simulation of a thin accretion disc around a black hole [16]. The colour coding shows the temperature at the surface of the disc. The null geodesics are computed for the Schwarzschild metric, any gravitational influence of the disc itself is neglected.

The hydrodynamical SPH simulation has been performed in a completely non-relativistic environment, i.e. using a Newtonian gravitational field for the dynamics of the disc. Self-gravitation of the disc is neglected completely. The major problem in doing a relativistic simulation is not that the hydrodynamics equations become more complicated on a relativistic background, but rather the fact that no covariant definition of viscosity exists [17].

As a complementary approach, one may turn to a geometry which has only the rotating disc itself as a source. We use the general relativistic rigidly rotating disc of dust as a simplified model of an accretion disc. For this model, a solution in terms of ultraelliptic functions is available [18]. The ray-tracing implementation [19] is used for the disc visualization in this paper.

With Weyl–Papapetrou coordinates (ρ, ζ, ϕ, t), the metric of the rigidly rotating disc of dust reads

$$(g_{ij}) = \begin{pmatrix} e^{2(k-U)} & 0 & 0 & 0 \\ 0 & e^{2(k-U)} & 0 & 0 \\ 0 & 0 & -a^2 e^{2U} + \rho^2 e^{-2U} & -a e^{2U} \\ 0 & 0 & -a e^{2U} & -e^{2U} \end{pmatrix}.$$

The resulting field equations are equivalent to the Ernst equation

$$\Re f \left(f_{,\rho\rho} + f_{,\zeta\zeta} + \frac{f_{,\rho}}{\rho} \right) = f_{,\rho}^2 + f_{,\zeta}^2,$$

where $\Re f$ denotes the real part of the Ernst potential f defined as

$$f = e^{2U} + i b \quad \text{with} \quad b_{,\zeta} = \frac{e^{4U}}{\rho} a_{,\rho}, \quad b_{,\rho} = -\frac{e^{4U}}{\rho} a_{,\zeta}.$$

The remaining metric function k can be calculated from the functions U and a by quadratures. In the approach via ultraelliptic functions [18], the Ernst potential depends on μ, which is defined by the radius ρ_0 of the disc and the angular velocity Ω:

$$\mu = 2\Omega^2 \rho_0^2 e^{-2V_0} \quad \text{with} \quad V_0(\mu) = U(\rho = 0, \zeta = 0; \mu),$$

with $\mu \in (0, \mu_0)$, $\mu_0 = 4.62966\ldots$. The Newtonian limit corresponds to $\mu \ll 1$, whereas the Kerr space-time is obtained for the extreme case $\mu \to \mu_0$ and $\rho_0 \to 0$.

Figure 23 shows an abstract visualization of the rotating disc of dust with varying value μ. The geometry of the disc is textured with two different, simplified images: a pie-like image with bluish colours on the top and another pie-like image with greenish colours on the bottom. The virtual camera is located at a position away from the disc, in almost flat space-time. The disc is viewed from slightly above. At a small value of μ, such as $\mu = 0.2$, only minor visual distortions appear. As μ increases, the distortions become more prominent. For example, both the bottom and the top of the disc are visible for $\mu = 0.8$ because of gravitational light bending. For larger μ, even several 'copies' of the top and bottom textures occur since light paths may orbit the disc several times. In addition, rotational distortions within the textures appear due to frame dragging.

Figure 24 extends the visualization to a more realistic model of the texture. The colour coding on the texture represents the temperature of the disc. The disc texture is the same as the one used in figure 22, with the SPH solution being mapped onto the geometry of the rigidly rotating disc of dust. Therefore, the space-times for SPH simulation and ray tracing are not
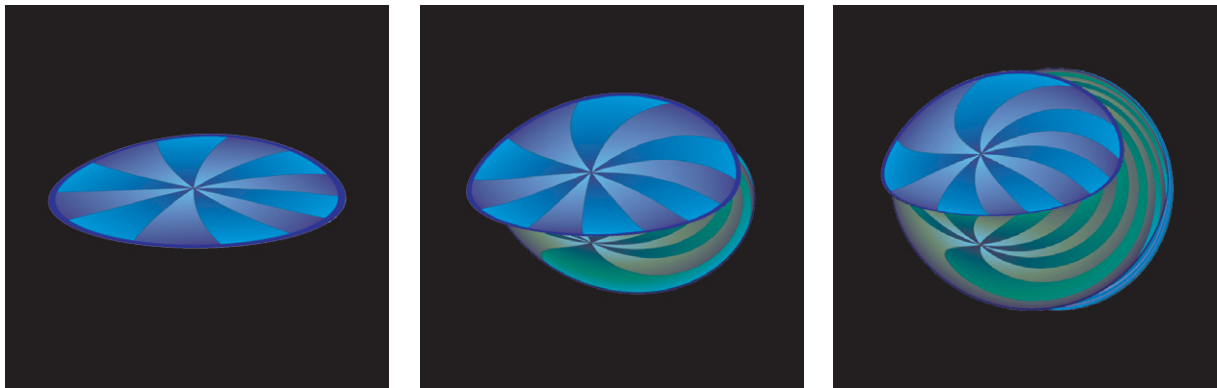
Figure 23. Abstract visualization of the rotating disc of dust with varying value $\mu = 0.2, 0.8, 1.5$ (from left to right).
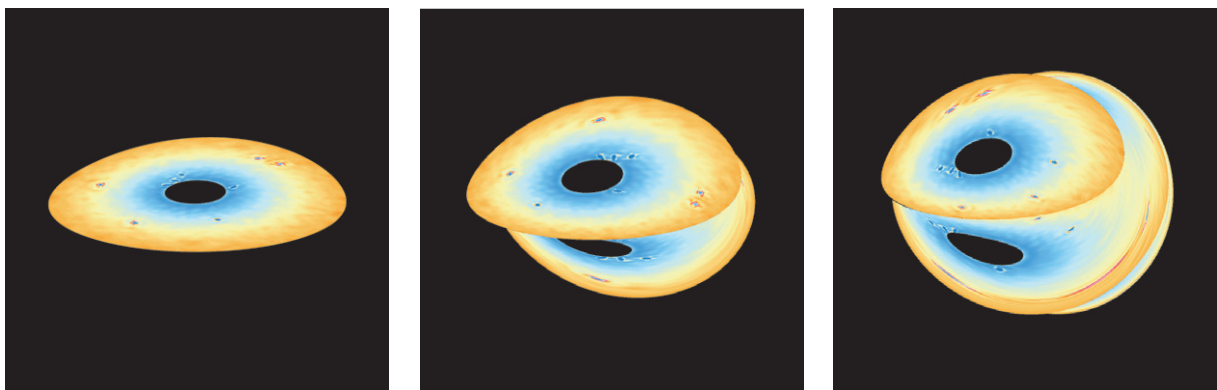

Figure 24. Visualization of the simplified model of an accretion disc around a black hole: the colour-encoded temperature distribution originates from an SPH simulation; this SPH solution is mapped onto the geometry of the rigidly rotating disc of dust with varying value $\mu = 0.2, 0.8, 1.5$ (from left to right).

identical; nevertheless, this simplified model provides a coarse approximation of the visual look of a general relativistic accretion disc.

A major challenge in computing these visualizations lies in the necessity to use very small step size in solving the geodesic equation in some regions of the space-time. This problem may also occur for other geometries, e.g. the warp drive, if the transition between the interior and the exterior of the warp bubble is made very steep. These computations thus require an adaptive and rather fast solver for ordinary differential equations.

4. Technical and logistic challenges

Being ambitious to provide visualization which looks realistic, one faces many problems which are of a technical, rather than scientific, nature. Still, many of these are not easy to solve, and often one will need to compromise to arrive at a 'sufficiently' realistic visualization with reasonable effort. We describe here some of the most vexing problems one may encounter.
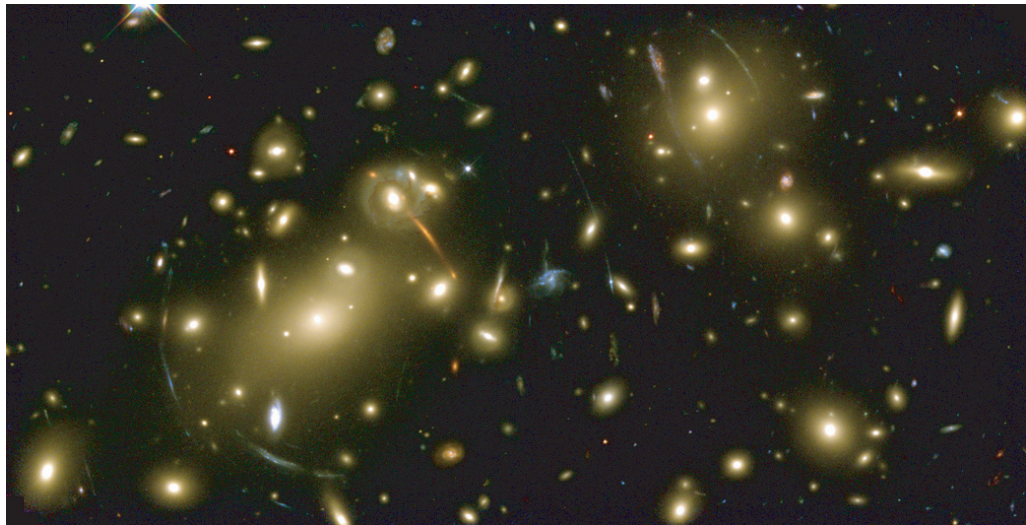
Figure 25. The gravitational field of the massive galaxy cluster Abell 2218, located about two billion light-years from the Earth, deflects light rays passing through it. It distorts images of objects further away and even acts as a magnifying lens for viewing distant galaxies that could not be observed otherwise. Image courtesy of NASA, Andrew Fruchter and the ERO Team (Sylvia Baggett (STScI), Richard Hook (ST-ECF) and Zoltan Levay (STScI)) [20].

We have seen that both in special and general relativistic visualization all of the surrounding scenery may become visible to an observer even if the field of view is limited. Therefore, complete image data of the whole surrounding scenery must be available. This can be achieved in two ways, by using a 3D model or by providing 4π panoramic images centered on the observer.

Constructing a detailed 3D model can be a daunting task: collecting the data for the model of the old city of Tübingen, which we have presented here, took several years! [8]. For single still images, working from 4π panoramic images is much easier. For movies, however, an individual panoramic image has to be provided for every frame of the movie. Interactive simulations generally cannot be done in this way since the user may choose any location within the scene.

These problems can be avoided if all the objects are considered to be infinitely far away, i.e. far compared to their own size and to a typical scale of the geometry under study. In this case, all the image data may be mapped onto a sphere at infinity. Only one panoramic image is necessary in this case, and the path of the observer relative to the geometry may be chosen arbitrarily.

Locating all objects infinitely far away, in the part of a space-time which is usually assumed to be asymptotically flat, also has the advantage that one does not need to worry about how the scenery itself would be affected by the geometry. Few of the buildings on the Tübingen marketplace would manage to remain standing upright if a wormhole of the same size as in figure 19 were placed as closely as shown in our pictures!

In astronomical situations the assumption that the objects we are looking at are very far away can usually be justified. However, this leads to another problem: even for the largest

telescopes that have been built or will be built in the foreseeable future, stars are essentially point-like objects. For various reasons they always appear as circular discs with finite radii on any actual picture. If such an image is used as the backdrop image for, say, a black hole geometry, then these discs will be elongated; even strongly so if the light rays pass close to the circular photon orbit. In reality, the stars, having a finite radius, would also appear as elongated discs. However, even these elongated discs would still be point-like to any telescope. The mechanisms turning points into circular discs in the picture-taking apparatus still operate the same, so these stars would still appear as circular discs on the picture, not as elongated discs.

Galaxies, nebulae, and any other object which can be resolved as extended by a telescope, on the other hand, will indeed become elongated on a picture taken in such a situation. This effect can be observed in reality, as a result of gravitational lensing as in figure 25. In fact, several examples of complete Einstein rings have been found by the Hubble space telescope [21].

In order to treat point-like and extended objects correctly in a simulation, one would have to distinguish between them on the original picture, and then process them differently—a very demanding task. You can see the distorted representation of stars in the picture of the warp bubble (figure 20, right panel).

Acknowledgments

References

[1] Einstein A 1917 *Über die spezielle und die allgemeine Relativitätstheorie gemeinverständlich* (Braunschweig: Vieweg) (in German)
Einstein A 1920 *Relativity, the Special and the General Theory: A Popular Exposition* (London: Methuen)
[2] Kornblum H W 1922 *Die Grundlagen der Einsteinschen Relativitätstheorie* (movie, in German) manuscript by Buek O, Fanta O, Lämmel R and Nicolai G F
Fleischer D 1923 *The Einstein Theory of Relativity* (movie)
[3] Benger W, Hege H-Ch and Heusler S 2000 *Visions of Numerical Relativity 1999. Appeared in: Science and Art Symp. 2000, 3rd Int. Conf. on Flow Interactions of Science and Art* (*ETH Zürich, 28 February–3 March 2000*) ed A Gyr *et al* (Dordrecht: Kluwer) pp 239–46
[4] Minkowski H 1908 Die Grundgleichungen für die elektromagnetischen Vorgänge in bewegten Körpern *Nachr. Ges. Wiss. Göttingen* 53–111 (in German)
[5] Diepstraten J, Weiskopf D and Ertl T 2002 Automatic generation and non-photorealistic rendering of 2 + 1D Minkowski diagrams *WSCG Conf. Proc.* pp 139–46
[6] Savage C M, Searle A and McCalman L 2007 *Am. J. Phys.* **75** 791
[7] Weiskopf D *et al* 2006 Explanatory and illustrative visualization of special and general relativity *IEEE Trans. Vis. Comput. Graphics* **12** 522–34
[8] http://www.kyb.mpg.de/bu/projects/vrtueb/ctuebindex.html (accessed 30 October 2008)
[9] Kraus U and Borchers M 2005 Fast lichtschnell durch die Stadt *Phys. Unserer Zeit* **2** 64–9 (in German)
http://www.spacetimetravel.org/tuebingen/tuebingen.html (English version) (accessed 30 October 2008)
[10] Nollert H-P, Ruder H and das Visualisierungsteam des SFB382 2005 Dierelativistische Welt in Bildern *Spektrum der Wissenschaft Spezial* **3** (in German)

[11] http://www.einsteinmobil.de/unterrichtsmodule/flugsimulator.html (accessed 30 October 2008)

[12] Morris M S and Thorne K S 1988 Wormholes in spacetime and their use for interstellar travel: a tool for teaching general relativity *Am. J. Phys.* **56** 395–412

[13] Alcubierre M 1994 The warp drive: hyper-fast travel within general relativity *Class. Quantum Grav.* **11** L73–7

[14] Müller Th 2004 Visual appearance of a Morris–Thorne-wormhole *Am. J. Phys.* **72** 1045–50

[15] Teo E 1998 Rotating traversable wormholes *Phys. Rev.* D **58** 024014

[16] Speith R 2007 Improvements of the numerical method Smoothed Particle Hydrodynamics *Habilitation* Eberhard-Karls-Universität Tübingen

[17] Carter B and Chamel N 2005 Covariant analysis of Newtonian multi-fluid models for neutron stars: III. Transvective, viscous, and superfluid drag dissipation *Int. J. Mod. Phys.* D **14** 749–74

[18] Neugebauer G and Meinel R 1995 General relativistic gravitational field of a rigidly rotating disk of dust: solution in terms of ultraelliptic functions *Phys. Rev. Lett.* **75** 3046–7

[19] Weiskopf D and Ansorg M 2000 Visualization of the general relativistic rigidly rotating disk of dust *Ann. Phys. Lpz.* **9** SI179–85

[20] http://hubblesite.org/newscenter/archive/releases/2000/07/image/b/ (accessed 30 October 2008)

[21] http://hubblesite.org/newscenter/archive/releases/2005/32/image/a/ (accessed 30 October 2008)